TRENDS IN SCIENCES 2025; 22(10): 10552
https://doi.org/10.48048/tis.2025.10552 RESEARCH ARTICLE

Rapid Microwave-Assisted Synthesis of Fe/Co Bimetallic Metal-Organic Frameworks and Evaluating the Role of Coordinatively Unsaturated Sites for Selective CO_2 Capture

Thilina Rajeendre Katugampalage[1], Preeti Waribam[1], Chalita Ratanatawanate[2], Mehmood Shahid[3], Pakorn Opaprakasit[1], Wanida Chooaksorn[4] and Paiboon Sreearunothai[1,*]

[1]School of Integrated Science and Innovation, Sirindhorn International Institute of Technology, Thammasat University, Pathum Thani 10200, Thailand
[2]National Nanotechnology Center, National Science and Technology Development Agency, Pathum Thani 12120, Thailand
[3]Laboratory of Inorganic Materials for Sustainable Energy Technologies, Mohammed VI Polytechnic University (UM6P), Ben Guerir 43150, Morocco
[4]Department of Environmental Science, Faculty of Science and Technology, Thammasat University, Pathum Thani 10200, Thailand

([*]Corresponding author's e-mail: paiboon@siit.tu.ac.th)

Received: 4 May 2025, Revised: 31 May 2025, Accepted: 10 June 2025, Published: 30 July 2025

Abstract

In this study, a novel CO_2 adsorbent was synthesized using a rapid microwave-assisted process, combining iron and cobalt metal ion precursors with terephthalic acid. A spindle-shaped bimetallic MOF sorbent with a crystal structure similar to MIL-88B was observed. The properties of the bimetallic MOFs were studied in comparison with their monometallic equivalents, and the mixed-metal MOFs showed a higher surface area and greater CO_2 adsorption capabilities. X-ray photoelectron spectroscopy studies revealed the presence of both bi- and trivalent ions, although only Fe^{3+} and Co^{2+} were used in the synthesis. Furthermore, the bimetallic MOFs exhibited coordinatively unsaturated metal sites, as evidenced by the acid-base titrations. Structural defects from incomplete coordination due to rapid synthesis and mixed-valence metal ion substitutions led to strong acidity. As a result, the bimetallic adsorbent exhibited a CO_2 adsorption capacity of 1 mmol g^{-1} with a 40-fold selectivity of CO_2 over N_2 under ambient conditions. The synthesis of adsorbents via the microwave process provides an energy-efficient pathway to produce MOFs with abundant active sites for selective CO_2 capture.

Keywords: Metal-organic frameworks, Microwave synthesis, CO_2 capture, High selectivity, Coordinatively unsaturated metal sites

Introduction

Anthropogenic carbon dioxide (CO_2) emissions have increased global atmospheric CO_2 concentration to an annual average of 419 ppm in 2022/2023, corresponding to a rise in global mean surface temperature of 1.1 °C [1]. As predicted, the atmospheric CO_2 concentration will increase significantly in the following decades with the increase in global energy consumption. Researchers are developing various methods that could be used to minimize this phenomenon, where direct air capture (DAC) is considered one of the promising technologies that can be scaled up to achieve net negative CO_2 emissions, possibly in the near future. Scalable, non-toxic, energy-efficient, and sustainable materials that are appropriate for large-scale carbon capture plants are crucial for CO_2 capture at ambient pressure. Metal-organic frameworks

(MOFs) are one of the well-studied materials for CO_2 sorption and have outperformed most traditional sorbents, indicating their potential to be utilized in large-scale applications [2].

Metal-organic frameworks are a unique category of highly porous materials, formed by coordinating metal ion clusters (secondary building units -SBUs) with organic linkers. These highly ordered porous structures create one-, two-, or three-dimensional networks with various physicochemical properties. The crystalline structure and porosity of the MOFs can be varied by choosing different types of metal ions and organic linkers [3]. MOFs are used in various applications owing to their advantageous properties, including high surface area and tunable structure. Due to their highly porous nature, high surface area, and framework flexibility, MOFs have been extensively used in CO_2 capture applications. ZIF-8 [4], IRMOF-1 [5], and MIL-101 [6] are among the few materials well-studied for their CO_2 sorption properties, with sorption capacities of 0.84, 1.92 and 1.60 mmol g^{-1}, respectively. Various strategies have been employed to enhance the CO_2 adsorption performance of MOFs, including linker modification and the use of modulators to introduce structural defects. These modifications, including introducing binary metal ions, have not only increased CO_2 uptake but also contributed to improved structural stability of the MOF candidates [7]. Mg-MOF-74 is one of the top-performing MOFs, which has shown reduced CO_2 uptake properties due to the structural compensation via competitive coordination of water molecules in the coordinatively unsaturated sites [8]. The moisture stability of Mg-MOF-74 has been improved by incorporating a second metal ion, such as Co^{2+} and Ni^{2+}, which are stable in moisture conditions, unlike Mg^{2+} [9].

Hence, our interest is in using bimetallic MOFs, as they have shown impressive performance in gas sorption, compared to monometallic MOFs. Introducing a secondary metal ion into the SBUs leads to defects in the MOF framework, arising from differences in the radius or charge of the newly added metal ions, forming coordinatively unsaturated metal sites (CUS) in the framework. The CUS plays a vital role in CO_2 adsorption in MOFs, being the primary coordination site for guest molecules. Among various reported materials, Mg/DOBC MOF is an interesting example of MOFs that possess coordinatively unsaturated sites (CUS) or open metal sites (OMS) in its structure [7]. The CPO-27-M MOF series, containing a large number of OMSs, has demonstrated excellent CO_2 adsorption properties of approximately 25-30 wt% CO_2 at elevated temperatures of 437 K [10]. MOFs with OMSs or Lewis's acid sites interact with CO_2 molecules due to the partial positive charges on the uncoordinated metal centers [11]. The study carried out by Yazaydın *et al*. [12] by screening 14 different MOFs for CO_2 capture from flue gas at low pressure (0.1 bar), suggested that the observed higher CO_2 adsorption capacity is due to the higher density of coordinatively unsaturated sites in the MOF structure. It was further stated that the improved CO_2 adsorption properties and conversion capability in Cu-based mixed metal MOFs were also due to the numerous OMSs [13]. Hence, it is clear that the enhanced adsorption capacity of CO_2 is caused by forming potent and selective interactions between the host structure and the CO_2 via coordinatively unsaturated sites. The MIL-88 series has garnered our interest due to its flexible framework and the potential to introduce coordinatively unsaturated sites into the structure through cluster modification. Moreover, most of the reported studies have focused on enhancing the BET surface area or incorporating functional groups to improve CO_2 uptake capacity, while relatively few have concentrated on improving the sorption capabilities of MIL-88B through the introduction of heterometallic SBUs.

This work focuses on the CO_2 adsorption properties of bimetallic Fe/Co MOFs synthesized by a microwave-assisted solvothermal route compared to their monometallic equivalents. Furthermore, the study investigates the role of coordinatively unsaturated sites in CO_2 selectivity over N_2 gas in the synthesized MOFs. The bimetallic MOFs were characterized using FTIR, XRD, TEM, FE-SEM, and XPS to determine the chemical and physical properties. Furthermore, the N_2 adsorption properties at 77 K and acid-base titrations were conducted to understand the porosity and coordinatively unsaturated sites, respectively. The CO_2 adsorption tests were conducted at room temperature from 0-1 bar pressure to determine the adsorption capacity and selectivity over N_2. Furthermore, the bimetallic MOF underwent heat treatment at high temperatures to destabilize the framework, and CO_2 adsorption was performed to validate the significance of

the CUS and the well-defined framework for gas adsorption. Therefore, this study provides a fast and energy-efficient method to prepare heterometallic MOFs, which could enable large-scale production of active materials for selective CO_2 capture applications in various industries.

Materials and methods

Materials

The chemical used in this study was analytical-grade and used without any purification. Iron(III) chloride hexahydrate ($FeCl_3 \cdot 6H_2O$, >= 99 %), cobalt(II) chloride tetrahydrate ($CoCl_2 \cdot 4H_2O$, 98-102 %), sodium hydroxide pellets (NaOH, 98 %), methanol (CH_3OH, 99.9 %), N,N-dimethylformamide (DMF, 99.9 %), and sodium nitrate (99 %) were obtained from Carlo Erba Reagents, Italy. Concentrated hydrochloric acid (HCl-37 %) was purchased from Quality Reagent Chemicals, Malaysia, and 1,4-benzene dicarboxylic (BDC, 99+ %) linker was obtained from Thermo Scientific, USA.

Synthesis of metal-organic frameworks

The synthesis and optimization of bimetallic and monometallic MOFs have been reported in detail in our previous work [14]. In brief, 5 mmol of iron and cobalt metal ions were mixed with 5 mmol of terephthalic acid (BDC) linkers and 0.4 M Sodium hydroxide solution using DMF as the solvent. The bimetallic MOF was synthesized using optimized iron and cobalt metal salts in a 2/3 ratio, as established in our previous work. The reaction was conducted in a 100 mL Teflon-lined microwave reactor at 140 ºC for 20 min, where the ramp time was set to 10 min (maximum power of the microwave reactor was set to 500 W). **Figure 1** illustrates the arrangement of heterometallic clusters with BDC linkers in forming bimetallic MOFs via microwave-assisted synthesis. Further, the bimetallic MOF was heat-treated at different temperatures under a N_2 atmosphere, and its CO_2 adsorption properties were studied compared to the as-synthesized samples.

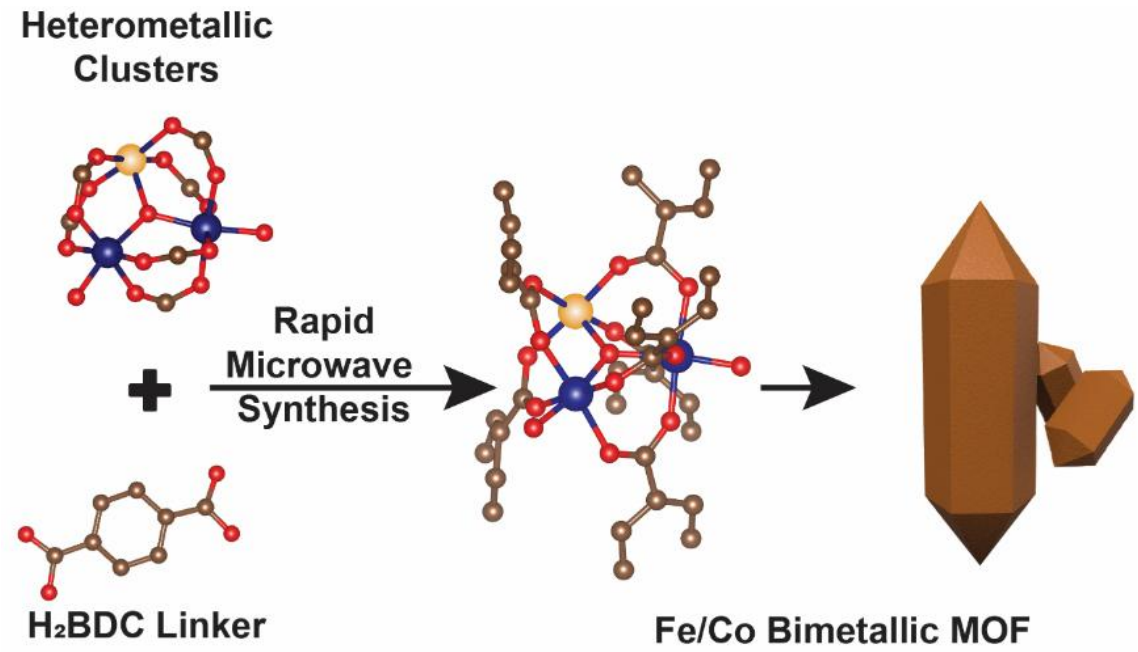

Figure 1 Illustration of the rapid microwave-assisted synthesis of bimetallic MOFs.

Characterizations of MOF

The crystal structures of the synthesized samples were examined using powder X-ray diffraction (PXRD), performed on a Bruker D8 Advance diffractometer (Bruker, Massachusetts, USA) equipped with a Cu-Kα radiation source (λ = 1.5406 Å), with a step size of 0.02°, operating at 40 kV and 40 mA. The morphology of the bimetallic MOFs was studied using TEM (Jeol TEM-2100Plus, Jeol Ltd., Tokyo, Japan) and FE-SEM (Hitachi FE-SEM model SU8030, Hitachi High-Tech, Tokyo, Japan). IR spectroscopy (ATR-FTIR) was conducted on all synthesized MOF samples, and

functional group analysis was carried out using (Nicolet iS5 - Thermo Scientific, Massachusetts, United States). X-ray photoelectron spectroscopy (XPS) was performed on a Kratos Analytical AXIS Supra instrument (AXIS Supra, Manchester, United Kingdom) using monochromatic Al Kα radiation at 225 W for high-resolution analysis. To determine the surface area and pore size, N_2 adsorption-desorption isotherms were measured at 77 K using a Micromeritics 3Flex (Micromeritics, Georgia, USA). Before the analysis, the samples were degassed at 150 °C for 12 h to remove any adsorbed species.

Room temperature CO_2 adsorption analysis

All the CO_2 adsorption analyses were carried out using Quantachrome Autosorb iQ-CMP gas adsorption analyzer. The CO_2 adsorption capacity between 0 - 1 bar of all synthesized MOFs was analyzed at 25 °C. Before the adsorption experiments, the samples were degassed at 100 °C for 2 h to remove any pre-adsorbed gases. Approximately 80 -100 mg of the synthesized MOF sorbent was used for each measurement. High-purity CO_2 (99.995 %) and N_2 (99.999 %) gases were employed to study the selective adsorption behaviour of the Fe/Co-BDC MOF. The selectivity factor from the single-component gas adsorption isotherms was calculated following the method described in our previous work [15].

Results and discussion

Physicochemical properties of the synthesized materials

Morphological analyses have been conducted on all synthesized samples to identify their distinctive microcrystalline structures. **Figure 2** shows the FE-SEM and TEM images of Fe/BDC, Co/BDC, and Fe/Co-BDC MOFs. Cobalt BDC MOFs were observed as 2D layers, similar to the $Co_2(OH)_2$BDC MOF structure reported [16]. The average size of the Co/BDC particles was larger than that of the bimetallic and monometallic counterparts. The shape of Co/MOF was a perfect 2D parallelogram of 2.8×1.9 µm in size. However, the Fe/BDC showed an irregular spherical shape where most particles were aggregated into several clusters. There was no evidence of the formation of spindle-shaped MIL-88B in the Fe/MOF sample. It was clear that a drastic morphological change occurred when Fe and Co were mixed, forming needle-shaped spindle-like microcrystals of MIL-88B. The crystal structure and nitrogen adsorption/desorption properties of the rapidly formed bimetallic MIL-88B sample were further studied to understand its porosity.

ATR-FTIR analysis was conducted initially to identify the coordination environment, as the formation of MOF occurs through the coordination between metal nodes and carboxylate group (-COO) of organic linkers. Successful coordination of the linker with Fe and Co metal ions could be observed from the ATR-FTIR spectra shown in **Figure 2.** (a) (red colour) showing the asymmetric (~1544 cm^{-1}) and symmetric stretching vibration (~1387 cm^{-1}) of -COO group of BDC linker. The difference (Δ) between the asymmetric and symmetric stretching frequencies (ν_{as} and ν_s) provided valuable insights into the coordination environment of the carboxylate groups (COO-) of the synthesized materials. The separation between the asymmetric and symmetric stretching bands in the Co/BDC MOF was around 220 cm^{-1}, similar to the vibrational splitting seen in the reported $Co_2(OH)_2$ BDC MOF featuring a two-dimensional layered morphology. The splitting reduced to approximately 190 cm^{-1} in the bimetallic sample, likely due to the coordination of BDC ligands with both iron and cobalt within a μ_3-oxo-centered SBU characteristic of MIL-88B, in contrast to the edge-sharing CoO_6 SBUs in the two-dimensional Cobalt MOF structure [14,17]. The observed shifts in the IR spectra indicate variations in the coordination environments of the synthesized MOFs, and PXRD patterns were analyzed subsequently to further understand their structural properties.

The crystal structures of Fe/Co-BDC, Fe/BDC, and Co/BDC MOFs are shown in **Figure 2** (**b**). The prepared Co/BDC MOF appeared to have characteristic diffraction patterns located at 2θ 8.8º, 14.1º, 15.8º º, 17.4º and 17.8º, which correspond well to the simulated pattern of layered Cobalt MOF reported by Kumroo *et al.* [18]. Fe/BDC MOF showed mixed phases of intermediate MOF-235 [19], and the presence of peaks at 24.2º, 33.1º and 35.6º confirms the formation of iron oxides (α-Fe_2O_3). Hence, it was clear that the short reaction time disfavours the formation of monometallic MIL-88B(Fe), due to the effect of $[FeCl_4]^-$ counter ion, which leads to the formation of MOF-235(Fe) [20]. In the bimetallic MOF sample containing both Fe and Co,

the diffraction pattern corresponded to that of MIL-88B, showing characteristic peaks at 2θ values of 8.8º, 9.3º, 10.5º, 16.7º, 18.6º and 20.8º [21]. The peaks observed at 9.3º, 10.5º, 16.7º, 18.6º and 20.8º correspond to the swollen or open phase of the MIL-88B, which is characterized by an increased unit cell volume. Moreover, the computational study on metal ligand covalency in the carboxylate ligands showed that the fraction of covalency increases as the oxidation state of the metal cation increases [22]. Since cobalt is in its 2+ state and Fe^{3+} is highly reactive, the second metal in the synthesis process has significantly influenced the formation of bimetallic MOFs. Hence, it was confirmed from the PXRD patterns that the bimetallic MOF has taken MIL-88B topology in a short reaction time.

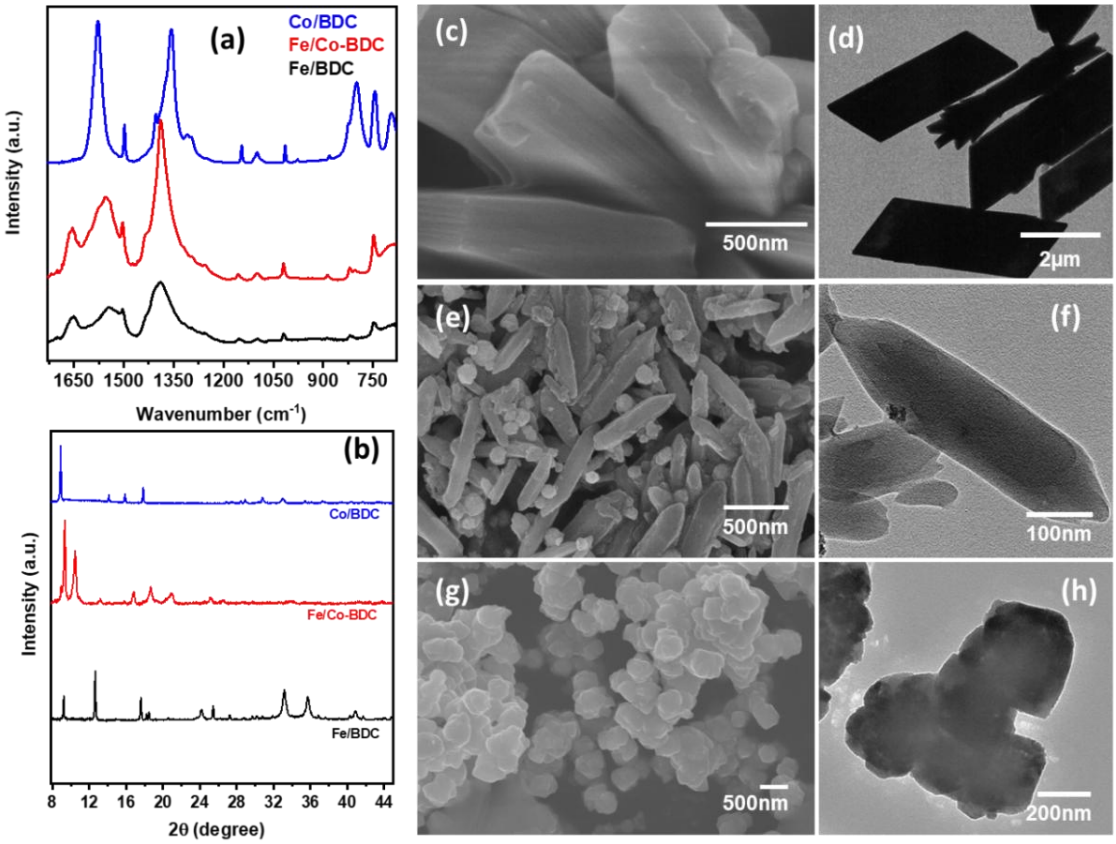

Figure 2 (a) FTIR spectra and (b) XRD patterns of Fe/BDC, Co/BDC, and Fe/Co-BDC MOFs. FE-SEM, TEM images of Co/BDC (c) and (d), Fe/Co-BDC (e) and (f), Fe/BDC MOF (g) and (h).

The microwave-assisted synthesis method produces MOFs in an energy-efficient way under a short reaction time, whereas solvothermal techniques generally take a few days. In a typical solvothermal setup, achieving high temperatures takes longer, thus consuming more energy. The rapid heating of the reaction mixture in a microwave setup, where energy is primarily absorbed by the solvents while the reactor remains unaffected, makes this method ideal for scaling up. Similarly, the synthesis of MIL-100 using the energy-efficient microwave approach has reduced its reaction time from 4 days to 4 h [23]. Unlike conventional heating, microwave heating is volumetric, enabling uniform reaction through the entire reaction volume, thus ideal for use in continuous flow tubular reactors. The reported work on Iron-based MIL-100 MOF was synthesized using a microwave-assisted continuous flow reactor, achieving a high space-time yield of ~771 kg/m^3/day [24], demonstrating the efficiency of the microwave-assisted technique. The synthesized MOFs were further characterized using nitrogen adsorption-desorption isotherms to gain insights into their porosity-related properties.

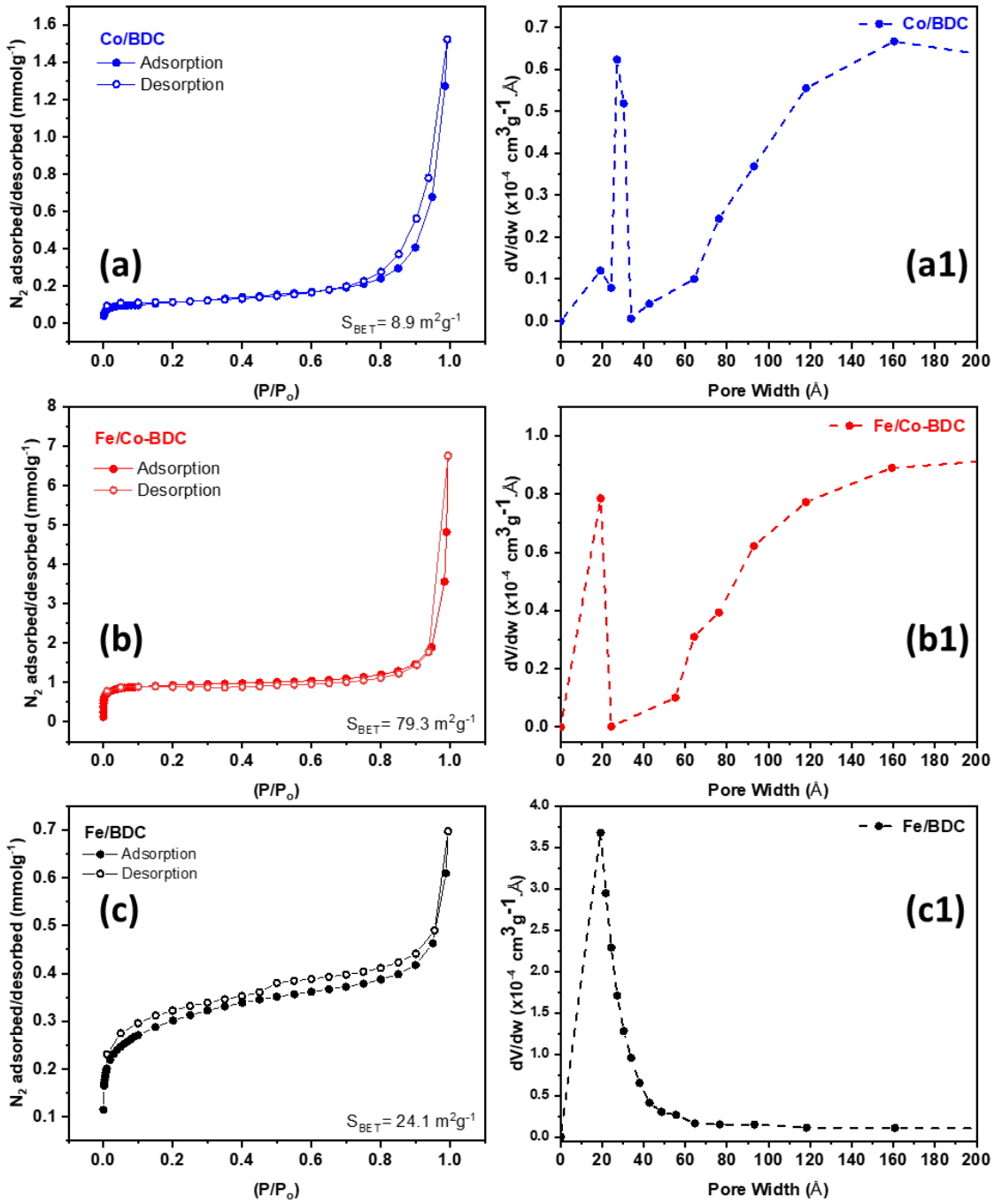

Figure 3 N_2 adsorption-desorption isotherm and pore size distribution. Co/BDC (a), (a1), Fe/Co-BDC (b),(b1) and Fe/BDC (c),(c1).

The surface area and pore size of the synthesized MOF materials were evaluated by N_2 adsorption-desorption isotherm experiments performed at 77 K. Co/BDC MOF, **Figure 3** (**a**) showed type IV isotherm with a hysteresis loop between 0.8 and 1, indicating the presence of mesopores, which corresponds with the study reported by Xuan *et al*. [25]. The Fe/BDC MOF, shown in **Figure 3** (**c**), exhibited the typical type I isotherm, indicating its microporous structure [26]. Interestingly, when Fe and Co metals are mixed, the bimetallic MOF showed the type I and type IV isotherms with a hysteresis loop, suggesting the presence of micropores as well as mesopores within the structure [27]. However, from the BJH pore size distribution shown in **Figures 3** (**a1**), (**b1**) and (**c1**), it was clear that Co/BDC showed the maximum pore size of ~2.71 nm and a pore size range between 6.44 and 16 nm, confirming the mesoporous nature. Monometallic

Fe/BDC showed very high microporosity with a pore size of 1.92 nm, and the Fe/Co-BDC MOF showed mixed pore size with ~1.92 nm and pores ranging between 6.42 - 16 nm, describing the presence of both micropores and mesopores. Although the surface area was not extensive, a notable enhancement was seen in the S_{BET} surface area of the bimetallic MOF (79.3 $m^2 g^{-1}$) compared to its monometallic variants (S_{BET} of 8.9 $m^2 g^{-1}$ - Co MOF and 24.1 $m^2 g^{-1}$ - Fe MOF). Hence, doping Fe with Co to create a heterometallic MOF has resulted in a material with unique mixed pore properties and high surface area, distinguishing it from monometallic MOFs. Therefore, the synthesized Fe/Co-BDC bimetallic MOF was further evaluated using XPS analysis.

XPS analysis

The metal nodes of the MOFs were characterized via X-ray Photoelectron Spectroscopy to gain more information about the binary metal ions and their valences. Wide scan XPS spectra of all synthesized MOFs show the presence of Fe and Co metal ions, C and O in the samples. The two spin-orbit components and satellite peaks were observed in the Fe 2p region, which was deconvoluted using the Gaussian fitting method (**Figures 4** (**b**) and (**c**)). The peaks correspond to 2p1/2, and Fe 2p3/2 were observed at 725.3 eV and 711.6 eV, indicating that the valence state of Fe was largely in the Fe^{III} state, considering the band separation of 13.4 eV [14,28,29]. The presence of Fe^{II} in the bimetallic MOF was evidenced by the peak shift observed towards the lower energy region with a slight shoulder, unlike its monometallic Fe/BDC sample. Therefore, the peak at 709.7 eV in the deconvoluted Fe 2p3/2 was attributed to Fe^{II}, while the peak at 711.6 eV was assigned to Fe^{III} [14,30].

The high-resolution Co 2p spectra were also deconvoluted using the Gaussian fitting method (**Figures 4** (**d**) and (**e**)), which identified 2 spin-orbit states along with 2 shakeup peaks. Peaks observed at 794.7 and 779.2 eV in both the cobalt-containing MOFs were ascribed to Co 2p1/2 and Co 2p3/2. The valence states of cobalt were identified by analyzing the difference in spin-orbit coupling values for Co 2p1/2 and Co 2p3/2, which was 15.5 eV, suggesting that both Co^{II} and Co^{III} coexist, even though only Co^{2+} ions were used during the synthesis [31]. Hence, the XPS analysis revealed that the secondary building units of the bimetallic MOFs contain both $Fe^{2+/3+}$ and $Co^{2+/3+}$, which could potentially result in structural mismatches within the framework during synthesis due to the competition between metal ions and ligands.

Acid-base titration of the synthesized MOFs

Morphological and physicochemical analysis of synthesized MOF samples evidence that the presence of hetero metal ions and rapid synthesis process could create favorable conditions for MOF formation with structural defects via mismatch during the synthesis. To gain further insights into these defective sites, an acid-base titration was conducted to identify the types of protons present in the synthesized MOF samples (**Figure 5**). The surface solid acid properties/Bronsted acidity was probed using acid-base titrations, where the acidity possibly could originate from the water molecules situated in the coordinatively unsaturated sites, structural hydroxyl groups, and hydroxyl groups stabilizing the MOF structure [32]. Two equivalence points were observed for Co BDC MOF measured at 0.8 ± 0.01 and 1.94 ± 0.01 with assigned pKa values at 4.2 and 7.7. Similarly, the equivalence points for Fe BDC MOF were measured at 0.7 ± 0.01 and 0.9 ± 0.01 with pKa values assigned at 3.3 and 3.6, respectively. Three major equivalence points were observed in the bimetallic MOF samples measured at 1.04 ± 0.01, 1.80 ± 0.01 and 2.18 ± 0.01 with pKa values assigned at 3.3, 4.1 and 5.0, respectively. The first pKa value observed for each MOF could be assigned to the μ_3-OH proton in the structure, and the common pKa value ~4 is most likely due to the uncoordinated -COOH terminals of the BDC linkers. The third observed proton presumably corresponds to defect sites in the MOF structure, which was observed only in the bimetallic MOF sample [33]. Hence, the three pKa values observed for the bimetallic MOF candidate could be attributed to μ_3-OH, -OH_2/-COOH, and -OH protons, whereas monometallic MOFs only observed the pKa values mainly corresponding to the μ_3-OH.

Moreover, we have observed that the bimetallic MOF sample acidifies neutral DI water to pH 4.2 upon incubation, a phenomenon consistently seen over 10 successive cycles. The strong bonding between coordinatively unsaturated sites/defective sites and μ_3-OH in the dispersed MOF solution can lead to the

detachment of a proton from water molecules, resulting in acidic aqueous solutions, which agrees with the results obtained from the acid-base titration. The Bronsted acidity was clearly evidenced with the presence of multiple equivalent points, resulting in three pK_a values for bimetallic MOF as shown in **Figure 5** (**b**), confirming the existence of coordinatively unsaturated metal sites due to the mismatch during the synthesis.

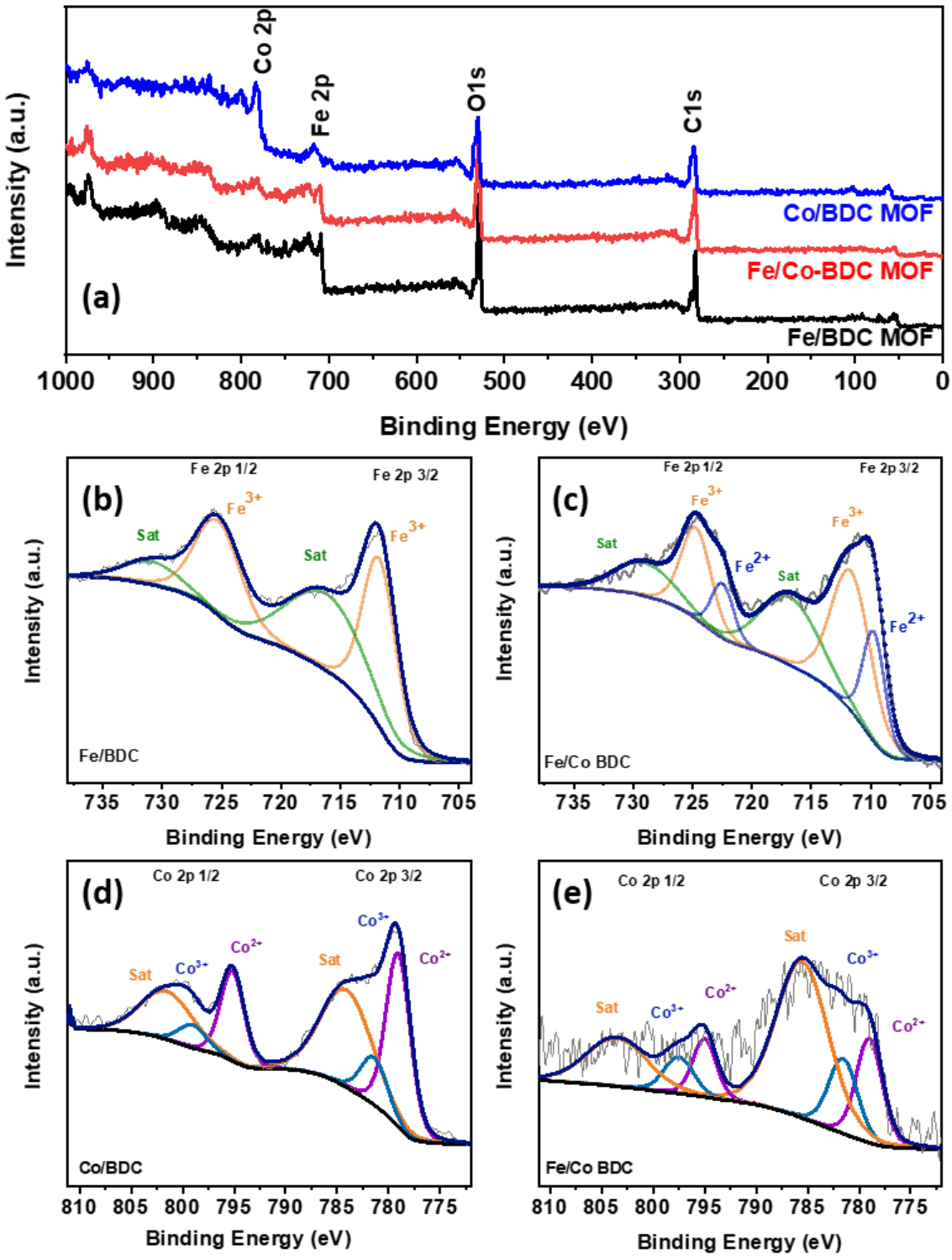

Figure 4 XPS analysis of monometallic Fe, Co MOFs, and bimetallic MOF - Fe 2p (b) and (c) and Co 2p (d) and (e).

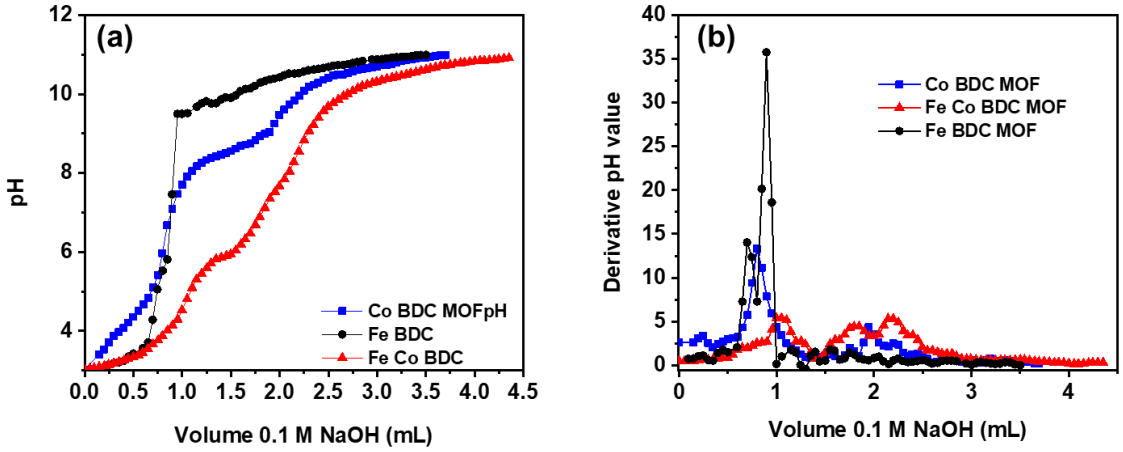

Figure 5 Acid-base titration curve of synthesized MOF materials (a), and first derivative curve (b) (0.01M $NaNO_3$ solution, 0.1M NaOH, 0.25 mg/mL MOF loading).

CO_2 adsorption properties and CO_2 selectivity over N_2

The CO_2 adsorption carried out at room temperature at low pressure between 0 to 1 bar is shown in **Figure 6** (**a**). It was noticed that the Fe/BDC and Co/BDC could absorb 0.39 and 0.11 mmol g^{-1}, respectively. However, a significant improvement was observed when Fe/Co-BDC MOF with 1 mmol g^{-1} CO_2 adsorption capacity, which was the highest among the synthesized samples. The higher CO_2 adsorption can be attributed to the strong electrostatic interactions between incoming CO_2 molecules and coordinatively unsaturated sites in the MOF structure observed in the synthesized bimetallic MOF [13]. Furthermore, this phenomenon was explained by L. Grajciar *et al.* [11] in their work on Cu-BTC MOF, where DFT and ab initio calculations were used. Grajciar concluded that the CO_2 adsorption on Cu-BTC MOF was due to the electrostatic interactions with the coordinatively unsaturated sites (or open metal sites) (Cu^{2+}) and the dispersion-driven interactions in the cage window sites. PDC Dietzel *et al.* have experimentally proven the direct interaction of CO_2 with nickel cations in the monometallic CPO-27-Ni framework via FTIR analysis [34]. Hence, the higher CO_2 adsorption capacity observed in Fe/Co MIL-88B of this work could also be attributed to open metal sites (OMS) and the OMS-driven larger cages in the structure. Furthermore, the multivalent species $Fe^{3+/2+}$ and $Co^{2+/3+}$ observed in the MOF structure can further generate defects or mismatches in the structure, resulting in larger cages due to the incompletely coordinated metal sites, which favor the adsorption of CO_2 molecules [35]. A similar phenomenon was observed in our previous work on defective UiO-66, where reo-defects played a significant role in CO_2 capture by stabilizing CO_2 within the confined pores [15]. Zhou *et al.* [36] further reported that the Mg metal sites in the bimetallic MIL-101(Cr,Mg) framework exhibit stronger interactions with CO_2 compared to the Cr sites, contributing to the higher CO_2 adsorption observed. When evaluating the Fe-MOF or the MOF-235 phase, we notice a lower CO_2 adsorption of 0.39 mmol g^{-1} due to the lack of unsaturated active sites. Thus, the defects in the bimetallic MOF directly contribute to its higher CO_2 adsorption capacity and increased selectivity. The selectivity of CO_2 over N_2 for Fe/Co-BDC MOF was studied considering a single gas component at 1.0 bar and 25 °C and calculated using the equation reported in our previous work, where the maximum quantity of CO_2 and N_2 (mmol g^{-1}) is considered at the relative pressure of 1 bar, respectively [15]. The equation for calculating CO_2 selectivity over N_2 is shown below. The obtained CO_2/N_2 selectivity was 40 times as shown in **Figure 6** (**b**), higher than some of the bimetallic MOF candidates reported by several researchers. The CO_2/N_2 selectivity of CuTMA(Co) and CuTMA(Fe) is about 16 times [13], while MOF-74(Ni) shows 27.6 times [37] at 1.0 bar pressure and 25 °C. This was mainly due to the contribution of the metal centers for the selective sorption, which can be attributed to the direct interaction of CO_2 with the metal cation framework.

$$\text{Selectivity factor} = \frac{q1/p1}{q2/p2} \quad (1)$$

In this expression, the maximum quantity of CO_2 and N_2 (mmol g^{-1}) adsorbed on the bimetallic MOF is represented by *q1* and *q2*, where *p1* and *p2* correspond to the partial pressures (bar) used for CO_2 and N_2 adsorption studied.

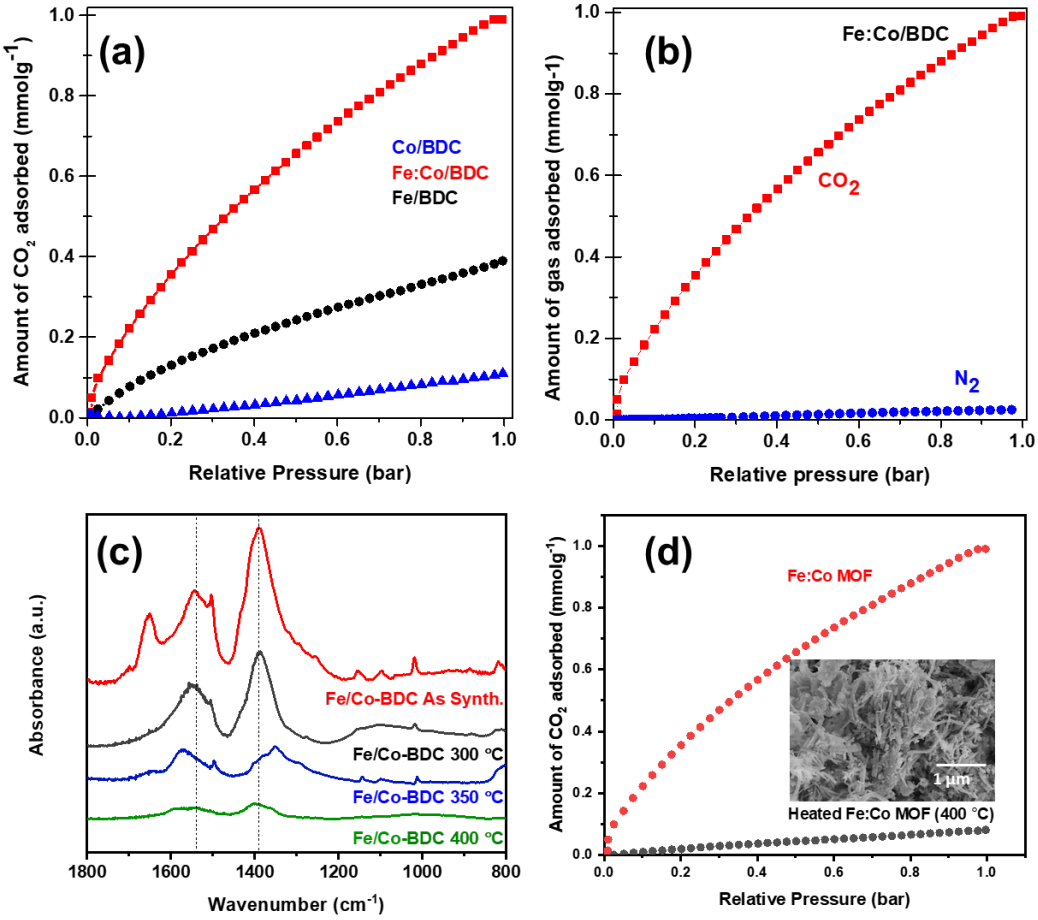

Figure 6 CO_2 adsorption of Co/BDC, Fe/Co-BDC and Fe/BDC MOF at 25 °C (a), CO_2/N_2 selectivity of Fe/Co bimetallic MOF (b), FTIR spectra of bimetallic MOFs heated at different temperatures (Heated under 20 ml/min of N_2 flow, 5 °C/min heating rate for 1 h) (c), CO_2 adsorption of Fe/Co-BDC MOF and the heated Fe/Co-BDC MOF (inset-FE-SEM image of heat treated bimetallic MOF at 400 °C) (d).

Moreover, the bimetallic MOF sample was then heated at elevated temperatures to destabilize the framework, turning it into carbon to understand the effect of coordinatively unsaturated sites and well-defined pores in the framework. The FTIR spectra of the MOF samples heat-treated at different temperatures were also collected and examined for the disappearance of the characteristic peaks of coordinated BDC linkers to confirm the framework disassembly (**Figure 6**. (**c**)). The CO_2 adsorption capacity of the destabilized/heated sample significantly decreased from 1 to 0.08 mmol g^{-1} (**Figure 6** (**d**)), further highlighting the importance of the coordinatively unsaturated sites and the well-defined pore structure of the MOF framework for CO_2 adsorption. In summary, the rapid synthesis has caused defect formation in the bimetallic MOF framework, while the presence of multivalent mixed metal ions further promotes the mismatch via competitive coordination. When the CO_2 and N_2 were introduced, the CO_2 interacted particularly with the open unsaturated metal centers, resulting in higher adsorption and selectivity.

Conclusions

This study demonstrates an efficient, rapid microwave-assisted synthesis of Fe/Co-BDC MOFs with a MIL-88B topology for CO_2 capture at ambient conditions. Reducing the synthesis time to under 20 min provides a scalable and energy-efficient approach to MOF production without compromising physicochemical properties. The microwave synthesis in this study consumes approximately 0.25 kWh per batch. In contrast, the solvothermal oven, rated at 3,000 W and assuming it operates at 50 % of its full power for about 2 days, consumes roughly 70 kWh per batch. The Fe/Co-BDC MOF features a high surface area and coordinatively unsaturated sites, which enhance CO_2 adsorption and selectivity, showing around 40 times higher affinity for CO_2 over N_2. The mixed-valent Fe and Co metal centers were unveiled via XPS analysis, and the acid-base titrations evidenced the defect-mediated CUS sites in the mixed metal MOF sample. The enhanced CO_2 adsorption capacity and selectivity over N_2 in bimetallic MOFs can be attributed to the strong electrostatic interactions between CO_2 molecules and the MOF framework. Therefore, the microwave-assisted synthesis approach presented in this work offers an energy-efficient and rapid method, showing strong potential for the large-scale production of materials aimed at industrial CO_2 capture. This study provides insights into the design of metal-organic frameworks (MOFs), particularly highlighting the role of heterometallic centers and coordinatively unsaturated sites in achieving selective CO_2 capture.

Acknowledgements

This research is supported by Thailand Science Research and Innovation (TSRI) Fundamental Fund, through Thammasat University, fiscal year 2569/2026. TK gratefully acknowledges the TU-NSTDA Excellent Research Graduate Scholarship (No. T2.1-6.-01) from the National Science and Technology Development Agency (NSTDA), Thammasat University, and the EFS Scholarship from Sirindhorn International Institute of Technology. PW gratefully acknowledges the Thammasat Postdoctoral Fellowship (TUPD 6/2567). Additional research support from Program Management Unit for Human Resources & Institutional Development, Research, and Innovation grant (no. B40G660035) and the Center of Excellence in Digital Earth and Emerging Technology (DEET), Thammasat University are also gratefully acknowledged.

Declaration of Generative AI in Scientific Writing

The authors acknowledge the use of generative AI tools built into Grammarly software for language editing and grammar correction in preparing this manuscript. No content generation or data interpretation was performed by AI. The authors take full responsibility for the content and conclusions of this work.

CRediT Author Statement

Thilina Rajeendre Katugampalage: Methodology, Conceptualization, Validation, and Writing original draft.

Preeti Waribam: Investigation, Validation, and editing original draft.

Chalita Ratanatawanate: Investigation and Resources.

Mehmood Shahid: Investigation, and Visualization.

Pakorn Opaprakasit: Resources and Funding acquisition.

Wanida Chooaksorn: Resources and Funding acquisition.

Paiboon Sreearunothai: Methodology, Project administration, Resources, Supervision, Validation, and Editing original draft.

References

[1] C Estruch, R Curcoll, JA Morgui, R Segura-Barrero, V Vidal, A Badia, S Ventura, J Gilabert and G Villalba. Exploring how the heterogeneous urban landscape influences CO_2 concentrations: The case study of the Metropolitan Area of Barcelona. *Urban Forestry & Urban Greening* 2024; **99**, 128438.

[2] X Zhang, H Zhao, Q Yang, M Yao, Yn Wu and Y Gu. Direct air capture of CO_2 in designed metal-organic frameworks at lab and pilot scale. *Carbon Capture Science & Technology* 2023; **9**, 100145.

[3] D Yuan, D Zhao, D Sun and HC Zhou. An Isoreticular Series of Metal-Organic Frameworks with Dendritic Hexacarboxylate Ligands and Exceptionally High Gas-Uptake Capacity. *Angewandte Chemie International Edition* 2010; **122(31)**, 5485-5489**.**

[4] J McEwen, JD Hayman and A Ozgur Yazaydin. A comparative study of CO_2, CH_4 and N_2 adsorption

in ZIF-8, Zeolite-13X and BPL activated carbon. *Chemical Physics* 2013; **412**, 72-76.

[5] KS Walton, AR Millward, D Dubbeldam, H Frost, JJ Low, OM Yaghi and RQ Snurr. Understanding Inflections and Steps in Carbon Dioxide Adsorption Isotherms in Metal-Organic Frameworks. *Journal of the American Chemical Society* 2008; **130**(**2**), 406-407.

[6] Y Lin, Q Yan, C Kong and L Chen. Polyethyleneimine Incorporated Metal-Organic Frameworks Adsorbent for Highly Selective CO_2 Capture. *Scientific Reports* 2013; **3**, 1859.

[7] CA Trickett, A Helal, BA Al-Maythalony, ZH Yamani, KE Cordova and OM Yaghi. The chemistry of metal-organic frameworks for CO_2 capture, regeneration and conversion. *Nature Reviews Materials* 2017; **2**, 17045.

[8] AC Kizzie, AG Wong-Foy and AJ Matzger. Effect of Humidity on the Performance of Microporous Coordination Polymers as Adsorbents for CO_2 Capture. *Langmuir* 2011; **27**(**10**), 6368-6373.

[9] L Chen, HF Wang, C Li and Q Xu. Bimetallic metal-organic frameworks and their derivatives. *Chemical Science* 2020; **11**(**21**), 5369-5403.

[10] PDC Dietzel, V Besikiotis and R Blom. Application of metal-organic frameworks with coordinatively unsaturated metal sites in storage and separation of methane and carbon dioxide. *Journal of Materials Chemistry* 2009; **19**(**39**), 7362-7370.

[11] L Grajciar, W Andrew D, PL Llewellyn, JS Chang and P Nachtigall. Understanding CO_2 Adsorption in CuBTC MOF: Comparing Combined DFT-ab Initio Calculations with Microcalorimetry Experiments. *The Journal of Physical Chemistry C* 2011; **115**(**36**), 17925-17933.

[12] AO Yazaydın, RQ Snurr, TH Park, K Koh, J Liu, MD LeVan, AI Benin, P Jakubczak, M Lanuza, DB Galloway, JJ Low and RR Willis. Screening of Metal-Organic Frameworks for Carbon Dioxide Capture from Flue Gas Using a Combined Experimental and Modeling Approach. *Journal of the American Chemical Society* 2009; **131**(51), 18198-18199.

[13] X He, DR Chen and WN Wang. Bimetallic metal-organic frameworks (MOFs) synthesized using the spray method for tunable CO_2 adsorption. *Chemical Engineering Journal* 2020; **382**, 122825.

[14] TR Katugampalage, P Waribam, P Opaprakasit, C Kaewsaneha, SH Hsu, W Chooaksorn, CA Jong, P Sooksaen, C Ratanatawanate and P Sreearunothai. Bimetallic Fe:Co metal-organic framework (MOF) with unsaturated metal sites for efficient Fenton-like catalytic degradation of oxytetracycline (OTC) antibiotics. *Chemical Engineering Journal* 2024; **479**, 147592.

[15] P Waribam, T Rajeendre Katugampalage, P Opaprakasit, C Ratanatawanate, W Chooaksorn, LP Wang, CH Liu and P Sreearunothai. Upcycling plastic waste: Rapid aqueous depolymerization of PET and simultaneous growth of highly defective UiO-66 metal-organic framework with enhanced CO_2 capture via one-pot synthesis. *Chemical Engineering Journal* 2023; **473**, 145349.

[16] Y Xu, B Li, S Zheng, P Wu, J Zhan, Xue, Q Xu and H Pang. Ultrathin two-dimensional cobalt-organic framework nanosheets for high-performance electrocatalytic oxygen evolution. *Journal of Materials Chemistry A* 2018; **6**(**44**), 22070-22076.

[17] GT Vuong, MH Pham and TO Do. Direct synthesis and mechanism of the formation of mixed metal Fe2Ni-MIL-88B. *CrystEngComm* 2013; **15**(**45**), 9694-9703.

[18] M Kurmoo, H Kumagai, M Green, B Lovett, S Blundell, A Ardavan and J Singleton. Two Modifications of Layered Cobaltous Terephthalate: Crystal Structures and Magnetic Properties. *Journal of Soli State Chemistry* 2001; **159(2)**, 343-351.

[19] Y Li, G Hou, J Yang, J Xie, X Yuan, H Yang and M Wang. Facile synthesis of MOF 235 and its superior photocatalytic capability under visible light irradiation. *RSC Advances* 2016; **6**(**20**), 16395-16403.

[20] D Bara, EG Meekel, I Pakamore, C Wilson, S Ling and RS Forgan. Exploring and expanding the Fe-terephthalate metal-organic framework phase space by coordination and oxidation modulation. *Materials Horizons* 2021; **8**(**12**), 3377-3386.

[21] GT Vuong, MH Pham and TO Do. Synthesis and engineering porosity of a mixed metal Fe2Ni MIL-88B metal-organic framework. *Dalton Transactions* 2013; **42**(**2**), 550-557.

[22] S Abednatanzi, PG Derakhshandeh, H Depauw, FX Coudert, H Vrielinck, PVD Voort and K Leus. Mixed-metal metal-organic frameworks. *Chemical Society Reviews* 2019; **48**(**9**), 2535-2565.

[23] RF Mendes, J Rocha and FAA Paz. Chapter 8 - Microwave synthesis of metal-organic frameworks, in: M. Mozafari (Ed.). *Metal-Organic Frameworks for Biomedical Applications Woodhead Publishing* 2020; **1**, 159-176.

[24] VN Le, HT Kwon, TK Vo, JH Kim, WS Kim and J Kim. Microwave-assisted continuous flow synthesis of mesoporous metal-organic framework MIL-100 (Fe) and its application to Cu(I)-loaded adsorbent for CO/CO_2 separation. *Materials Chemistry and Physics* 2020; **253**, 123278.

[25] W Xuan, R Ramachandran, C Zhao and F Wang. Influence of synthesis temperature on cobalt metal-organic framework (Co-MOF) formation and its electrochemical performance towards supercapacitor electrodes. *Journal of Solid State Electrochemistry* 2018; **22**, 3873-3881.

[26] WSA El-Yazeed, YGA El-Reash, LA Elatwy and AI Ahmed. Facile fabrication of bimetallic Fe-Mg MOF for the synthesis of xanthenes and removal of heavy metal ions. *RSC Advances* 2020; **10**(**16**), 9693-9703.

[27] A Benitez, J Amaro-Gahete, D Esquivel, FJ Romero-Salguero, J Morales and A Caballero. MIL-88A Metal-Organic Framework as a Stable Sulfur-Host Cathode for Long-Cycle Li-S Batteries. *Nanomaterials* 2020; **10**(**3**), 424.

[28] S Zhang, Y Zhuo, CI Ezugwu, CC Wang, C Li and S Liu. Synergetic Molecular Oxygen Activation and Catalytic Oxidation of Formaldehyde over Defective MIL-88B(Fe) Nanorods at Room Temperature. *Environmental Science & Technology* 2021; **55**(**12**), 8341-8350.

[29] H Lv, H Zhao, T Cao, L Qian, Y Wang and G. Zhao. Efficient degradation of high concentration azo-dye wastewater by heterogeneous Fenton process with iron-based metal-organic framework. *Journal of Molecular Catalysis A: Chemical* 2015; **400**, 81-89.

[30] J Zhu, X Lu, J Zhang, H Sun, C Zhang, Z Jiang, C Ju, Z Wang, F Huang and J Zhu. The effect of Fe^{2+} ions on dielectric and magnetic properties of $Yb_3Fe_5O_{12}$ ceramics. *Journal of Applied Physics* 2012; **111(1)**.

[31] A Indra, PW Menezes, I Zaharieva, H Dau and M Driess. Detecting structural transformation of cobalt phosphonate to active bifunctional catalysts for electrochemical water-splitting. *Journal of Materials Chemistry A* 2020; **8**(**5**), 2637-2643.

[32] W Liang, L Li, J Hou, ND Shepherd, TD Bennett, DM D'Alessandro and V Chen. Linking defects, hierarchical porosity generation and desalination performance in metal-organic frameworks. *Chemical Science* 2018; **9**(**14**), 3508-3516.

[33] RC Klet, Y Liu, TC Wang, JT Hupp and OK Farha. Evaluation of Brønsted acidity and proton topology in Zr- and Hf-based metal-organic frameworks using potentiometric acid-base titration. *Journal of Materials Chemistry* 2016; **4**, 1479-1485.

[34] PDC Dietzel, RE Johnsen, H Fjellvag, S Bordiga, E Groppo, S Chavan and R Blom. Adsorption properties and structure of CO_2 adsorbed on open coordination sites of metal-organic framework Ni2(dhtp) from gas adsorption, IR spectroscopy and X-ray diffraction. *Chemical Communications* 2008; **1**(**41**), 5125-5127.

[35] Y Abdoli, M Razavian and S Fatemi. Bimetallic Ni-Co-based metal-organic framework: An open metal site adsorbent for enhancing CO_2 capture. *Applied Organometallic Chemistry* (2019); **33**(**8**), 5004.

[36] Z Zhou, L Mei, C Ma, F Xu, J Xiao, Q Xia and Z Li. A novel bimetallic MIL-101(Cr, Mg) with high CO_2 adsorption capacity and CO_2/N_2 selectivity. *Chemical Engineering Science* 2016; **147**, 109-117.

[37] L Lei, Y Cheng, C Chen, M Kosari, Z Jiang and C He. Taming structure and modulating carbon dioxide (CO_2) adsorption isosteric heat of nickel-based metal organic framework (MOF-74(Ni)) for remarkable CO_2 capture. *Journal of Colloid and Interface Science* 2022; **612**, 132-145.